Ocean Dynamics (2003) 53: 11–20
DOI 10.1007/s10236-002-0021-8

Jin-Song von Storch

On the three-dimensional oceanic density distribution in a millennium integration with an AO-GCM

Received: 4 October 2001 / Accepted: 10 October 2002

Abstract The three-dimensional time-mean density distribution in the ocean is determined not only by the time-mean fluxes of heat and freshwater at the sea surface, but also by time-mean vertical currents and time-mean density fluxes due to oceanic transients excited by fluctuating fluxes at the sea surface. The effects of these various processes on the global density fields are assessed using a balance equation of the variance of spatial density anomalies and a millennium integration with an atmosphere–ocean general circulation model. It is found that spatial density anomalies are generated by the time-mean heat fluxes at the sea surface and destroyed by the time-mean surface freshwater flux, by sinking of dense water and rising of less dense water, and finally by density fluxes associated with transients. The last two processes take place essentially in the oceanic interior. Since density fluxes of transient eddies act to reduce the existing density differences between the Atlantic/Southern Oceans and the other oceans, their presence could affect the global density balance, and from that the thermohaline circulation and the stability of this circulation.

Keywords Time-mean density distribution · Transient eddies · ECHAM3-LSG integration

1 Introduction

The global density distribution directly affects the thermohaline circulation. If the northern North Atlantic were not that dense, and the Atlantic not denser than the Pacific and the Indian Ocean, there would be no overturning circulation in the Atlantic, and the global thermohaline "conveyor" circulation would not exist in its present form.

Responsible Editor: Richard J. Greatbatch

J. S. von Storch
Meteorologis des Institut des Universität Hamburg,
20146 Bundesstr. 55, Hamburg, Germany
e-mail: jin-song.storch@dkiz.de

One forcing for the global density distribution is the fluxes of heat and freshwater at the sea surface. The important role of these fluxes in determining the global thermohaline circulation has been extensively investigated. Some previous numerical studies showed that different thermohaline circulations exist, when the density of the water in the North Atlantic is lowered by adding extra amounts of freshwater (rain or river runoff). The sensitive dependence of the circulation on the freshwater forcing was further quantified in terms of hysteresis behavior (Stocker and Wright 1991; Rahmstorf 1995). The sensitivity originates from the two opposing effects of the heat and freshwater fluxes, which were considered by Stommel (1961) more than 40 years ago. The time-mean heat flux is associated with a stronger heating in the lower than in the higher latitudes. Thus, it tends to increase the latitudinal temperature contrast, and from that the latitudinal density difference. The time-mean freshwater flux, on the other hand, is associated with an excess of evaporation over precipitation in the subtropics and an excess of precipitation over evaporation in the polar regions. It tends to make the subtropics more saline than the polar regions, and hence to reduce the latitudinal density difference. The stability of the thermohaline circulation depends crucially on the balance of these two opposing surface forcings.

The heat and freshwater fluxes at the sea surface are, however, not the only forcing responsible for the three-dimensional density distribution and the ensuing thermohaline circulation. There are at least two other processes capable of affecting the density fields. One is related to vertical motions. Vertical motions stabilize (destabilize) a water column through downward movements of dense (light) water and upward movements of light (dense) water. From an energetic point of view, this process is related to the conversion between kinetic and potential energy.

Another process capable of affecting the three-dimensional density distribution is related to density fluxes induced by transient eddies. Generally, transient oceanic eddies can form non-zero time-mean density fluxes, in

analogy to atmospheric transients which result in non-zero heat fluxes. In the atmosphere, heat fluxes due to transients systematically transport heat poleward, thereby reducing the latitudinal temperature gradient and making the atmosphere more stable. In the ocean, the effect of transients on the thermohaline circulation, due to the lack of three-dimensional data, is essentially unknown. The situation is also more complicated than in the atmosphere. Oceanic transients can be produced both internally through instability processes, as in the atmosphere, and externally through fluctuating fluxes at the sea surface. The effect of the former on the three-dimensional density distribution and the consequent thermohaline circulation has to be studied using an eddy-resolving model of global oceans. This requires heavy computations and will not be considered here. The latter can be obtained using a present-day global atmosphere–ocean general circulation model (AO-GCM). Such a model generally contains a coarse-resolution oceanic GCM, which, when driven by climatological fluxes, produces little internal variability, and an atmospheric GCM, which resolves the major part of atmospheric eddies (i.e., synoptic variations). Within such a coupled model, no matter whether or not the oceanic component alone produces variations, the fluctuating fluxes could act as a stochastic forcing and excite additional variations (Hasselmann 1976). The effect of these externally excited variations on the mean density distribution can then be studied using an integration obtained from the coupled model.

The purpose of this paper is to assess the effects of the time-mean fluxes of heat and fresh-water at the sea surface and the above-mentioned two processes in generating or destroying spatial density anomalies. A millennium integration of the ECHAM3-LSG GCM (Voss 1996; Voss et al. 1998) is considered for this purpose.

The atmospheric part of the coupled model is the ECHAM3 model in T21 resolution. It resolves the major atmospheric eddies. The oceanic component is the LSG model (Maier-Reimer et al. 1993). It is based on the hydrostatic and Boussinesq approximations plus a further simplification which neglects the advection in the momentum equations. The LSG model has an effective resolution of about 4° latitude by 4° longitude. The ECHAM3-LSG GCM and the performance of this model in simulating oceanic circulation are described by Voss (1996) and von Storch et al. (2000). The LSG model does not resolve oceanic eddies and will produce an essentially stationary solution when driven by steady surface forcing. Oceanic variations in the coupled integration are therefore externally generated. Delworth and Greatbatch (2000) showed that the multidecadal thermohaline variations in their coupled GCM are essentially generated by surface heat flux forcing from the atmosphere. In the ECHAM3-LSG run, the externally generated variations reveal different spectral behavior (von Storch et al. 2001). While variations in the upper ocean are essentially white on time scales longer than one year, the spectral power of variations in the deep ocean increases with increasing time scales, suggesting pronounced variations on time scales of decades to centuries. The characteristics of these variations are comparable to those produced by other AO-GCMs (von Storch et al. 2000).

To assess the relative importance of processes responsible for the density distribution, an equation describing the maintenance of the variance of spatial density anomalies is given in Section 2. According to this equation, the contributions from four different processes are estimated using the ECHAM3-LSG integration in Section 3. Discussions and conclusions are given in the final section.

2 The balance equation

In the following, density ρ will be decomposed spatially and temporally into

$$\rho = \bar{\rho} + \rho' = [\bar{\rho}] + \bar{\rho}^* + \rho' \,, \tag{1}$$

where $^-$, $[\,]$, $'$ and * are operators which are applied on density ρ. $^-$ denotes the time mean and $[\,]$ is the area average defined by $[\,] = \frac{1}{A_z}\int_S \mathrm{d}S$ with A_z being the global oceanic area at a given depth z and $\int_S \mathrm{d}S$ being area integral. * and $'$ are deviations from the global area average and time mean. The quantity of special interest here is $\bar{\rho}^*$, which represents the time-mean spatial density anomalies (hereafter referred to as spatial density anomalies). It reflects important density features, such as the density contrast between the Atlantic and the Pacific and the density differences within the North Atlantic. The maintenance of spatial density anomalies is described by the balance equation of $\bar{\rho}^{*2}$, or the balance equation of

$$P_m = -\frac{1}{2}\int_V g\left(\frac{\delta[\overline{\rho_\theta}]}{\partial z}\right)^{-1}\bar{\rho}^{*2}\,\mathrm{d}V \,, \tag{2}$$

where $\int_V \mathrm{d}V$ indicates the volume integral over the oceans; g is gravity; ρ_θ is local potential density; $\frac{\delta[\overline{\rho_\theta}]}{\partial z}$ is related to the mean local static stability. The calculation of $\delta\rho_\theta$ is described below in Eq. (5). $-g\left(\frac{\delta[\overline{\rho_\theta}]}{\partial z}\right)^{-1}$ is a positive quantity and gives a stable layer more weight than a less stable layer. In the ECHAM3-LSG integration, the amplitude of $\frac{\delta[\overline{\rho_\theta}]}{\partial z}$ decreases with increasing depth in the upper 700 m and becomes very small below 1000 m. The profile suggests that the model oceans are statically most stable in the uppermost layer and almost neutral below 1000 m. $-\frac{1}{2}\int_V g\left(\frac{\delta[\overline{\rho_\theta}]}{\partial z}\right)^{-1}\bar{\rho}^{*2}\,\mathrm{d}V$ represents an approximative form of the available potential energy (Oort et al. 1989; Huang 1999).

If a process generates spatial density anomalies, no matter whether positive or negative, it will lead to an increase in $\bar{\rho}^{*2}$ and consequently an increase in P_m. If a process destroys spatial density anomalies, it will lead to a reduction in $\bar{\rho}^{*2}$ and P_m.

To obtain the balance equation of P_m, one needs to consider the density equation. In the LSG model, the prognostic variables are salinity, S, and potential temperature, θ. The model converts the latter to temperature T using $T = \theta + cz$ with c being a constant. The density is calculated using the UNESCO formulas (UNESCO 1981). At a given level, $\rho = \rho[T, S, p(z)]$, where $p(z)$ is a depth-dependent pressure. One has

$$\frac{\mathrm{d}\rho}{\mathrm{d}t} = \left(\frac{\partial p}{\partial \theta}\right)_{S,p} \frac{\mathrm{d}\theta}{\mathrm{d}t} + \left(\frac{\partial \rho}{\partial S}\right)_{\theta,p} \frac{\mathrm{d}S}{\mathrm{d}t} + \left(\frac{\partial \rho}{\partial z}\right)_{S,\theta} w \ . \tag{3}$$

Substituting the equations of θ and S (see Maier-Reimer et al. 1993) into Eq. (3), the density equation reads:

$$\frac{\partial \rho}{\partial t} = -\mathbf{v}_h \cdot \nabla_h \rho - w \frac{\delta \rho_\theta}{\partial z} + \frac{\mathcal{B}}{\Delta z_s} + A_d \left(\frac{\partial \rho}{\partial \theta}\right)_{S,p} \Delta\theta + A_d \left(\frac{\partial \rho}{\partial S}\right)_{\theta,p} \Delta S \ . \tag{4}$$

$\mathbf{v}_h$ is the horizontal velocity vector and ∇_h is the horizontal Nabla operator. In the derivation of Eq. (4), the following relation is used

$$\frac{\delta \rho_\theta}{\partial z} = \frac{\partial \rho}{\partial z} - \left(\frac{\partial \rho}{\partial z}\right)_{S,\theta} \ . \tag{5}$$

The quantity on the left-hand side equals $\delta\rho_\theta$ divided by ∂z where $\delta\rho_\theta$, at a level z, is the difference between potential densities in the neighboring layers (above and below z) referred to z and ∂z is the depth of the two neighboring layers. A_d is the diffusion coefficient. For the sake of simplicity, a distinction between vertical and horizontal diffusion is not made. The forcing, $\mathcal{B}$,

$$\mathcal{B} = \left(\frac{\partial \rho_s}{\partial \theta}\right)_{S,p} \frac{\mathcal{H}}{\rho_s c_w} - \left(\frac{\partial \rho_s}{\partial S}\right)_{\theta,p} S_s \mathcal{F} \tag{6}$$

occurs only in the surface layer, whose thickness is Δz_s. ρ_s is the density and S_s is the salinity at the sea surface. $\mathcal{H}$ and $\mathcal{F}$ are the downward fluxes of heat and freshwater.

When decomposing ρ_θ, ρ, and $(\frac{\partial \rho}{\partial z})_{S,\theta}$ in Eq. (5) temporally and spatially and applying the time and area average on the result, one obtains

$$\frac{\delta[\overline{\rho_\theta}]}{\partial z} = \frac{\partial[\bar{\rho}]}{\partial z} - \left[\overline{\left(\frac{\partial \rho}{\partial z}\right)_{S,\theta}}\right] \ . \tag{7}$$

Similar relations hold for the time (or area) averages of ρ_θ, ρ, and $(\frac{\partial \rho}{\partial z})_{S,\theta}$. Using these relations and the full Eq. (5), one finds furthermore

$$\frac{\delta \rho'_\theta}{\partial z} = \frac{\partial \rho'}{\partial z} - \left(\frac{\partial \rho}{\partial z}\right)' _{S,\theta} \tag{8}$$

and

$$\frac{\delta \overline{\rho_\theta}^*}{\partial z} = \frac{\partial \bar{\rho}^*}{\partial z} - \overline{\left(\frac{\partial \rho}{\partial z}\right)}^*_{S,\theta} \ . \tag{9}$$

Decomposing the variables in Eq. (4) temporally and spatially, multiplying the result with $\bar{\rho}^*$ and taking the time and area average, one obtains after making use of Eqs. (8)–(9),

$$\begin{aligned}\frac{\partial}{\partial t}\left[\frac{1}{2}\bar{\rho}^{*2}\right] = {} & \frac{[\bar{\rho}^* \bar{\mathcal{B}}^*]}{\Delta z_s} - [\bar{\rho}^* \bar{w}^*] \frac{\delta[\overline{\rho_\theta}]}{\partial z} + [\overline{\rho' \mathbf{v}'} \cdot \nabla_3 \bar{\rho}^*] \\ & \times \left[A_d \bar{\rho}^* \overline{\left(\frac{\partial \rho}{\partial \theta}\right)_{S,p} \Delta\theta} + A_d \bar{\rho}^* \overline{\left(\frac{\partial \rho}{\partial S}\right)_{\theta,p} \Delta S}\right] \\ & + \left[\bar{\rho}^* \bar{w} \overline{\left(\frac{\partial \rho^*}{\partial z}\right)}^*_{\theta,S}\right] + \left[\bar{\rho}^* w' \overline{\left(\frac{\partial \rho}{\partial z}\right)'}_{\theta,S}\right] \\ & - \left[\nabla_3 \cdot \left(\bar{\mathbf{v}} \frac{1}{2} \bar{\rho}^{*2}\right)\right] - \left[\nabla_3 \cdot \left(\bar{\rho}^* \overline{\mathbf{v}' \rho'}\right)\right] \ , \end{aligned} \tag{10}$$

where the fact, $\nabla_h[\bar{\rho}] = 0$, is used. $\mathbf{v} = \bar{\mathbf{v}} + \mathbf{v}'$ is the three-dimensional velocity vector and ∇_3 is the three-dimensional Nabla operator.

For each model layer, Eq. (10) is multiplied with $-g\left(\frac{\delta[\overline{\rho\theta}]}{\partial z}\right)^{-1} A_z \Delta z$ with Δz being the layer thickness. Integrating the result from the bottom layer to the surface layer and noting that $\int_z A_z[\,]\,\mathrm{d}z = \int_z \int_S \mathrm{d}s\,\mathrm{d}z$ equals $\int_V \mathrm{d}V$ and the volume integral of the last two terms in Eq. (10) vanishes, one obtains the equation of P_m

$$\frac{\partial P_m}{\partial t} = G1 + G2 + G3 + G4 + D = 0 \tag{11}$$

with

$$G1 = g\left(\frac{\delta[\overline{\rho_\theta}]}{\partial z}\right)_s^{-1} \frac{\alpha_o}{c_w} \int_s \bar{\rho}^*_s \bar{\mathcal{H}}^* \,\mathrm{d}S \tag{12}$$

$$G2 = g\left(\frac{\delta[\overline{\rho_\theta}]}{\partial z}\right)_s^{-1} \beta_o \rho_o S_o \int_s \bar{\rho}^*_s \bar{\mathcal{F}}^* \,\mathrm{d}S \tag{13}$$

$$G3 = g \int_V \bar{\rho}^* \bar{w}^* \,\mathrm{d}V \tag{14}$$

$$G4 = -g \int_V \left(\frac{\delta[\overline{\rho_\theta}]}{\partial z}\right)^{-1} \overline{\rho' \mathbf{v}'} \cdot \nabla \bar{\rho}^* \,\mathrm{d}V \tag{15}$$

$$\begin{aligned} D = {} & -\int_V g\left(\frac{\delta[\overline{\rho_\theta}]}{\partial z}\right)^{-1} \\ & \times \left[A_d \bar{\rho}^* \overline{\left(\frac{\partial \rho}{\partial \theta}\right)_{S,p} \Delta\theta} + A_d \bar{\rho}^* \overline{\left(\frac{\partial \rho}{\partial S}\right)_{\theta,p} \Delta S}\right] \mathrm{d}V \\ & - \int_V g\left(\frac{\delta[\overline{\rho_\theta}]}{\partial z}\right)^{-1} \bar{\rho}^* \bar{w} \overline{\left(\frac{\partial \rho}{\partial z}\right)}^*_{\theta,S} \mathrm{d}V \\ & - \int_V g\left(\frac{\delta[\overline{\rho_\theta}]}{\partial z}\right)^{-1} \bar{\rho}^* w' \overline{\left(\frac{\partial \rho}{\partial z}\right)'}_{\theta,S} \mathrm{d}V \ , \end{aligned} \tag{16}$$

where $\int_s \mathrm{d}S$ is the integral over the sea surface. Quantities denoted by the subscript $_o$ indicate constants. In the derivation of Eq. (12) and Eq. (13), it is assumed that the density at the sea surface depends linearly on temperature and salinity. Thus, $\frac{1}{\rho_s}\left(\frac{\partial \rho}{\partial \theta}\right)_{S,p}$ is approximated by $-\alpha_o$, $\left(\frac{\partial \rho}{\partial S}\right)_{\theta,p}$ by $\beta_o \rho_o$. S_s and the specific heat c_w in Eq. (6)

are assumed to be constant. We take $\alpha = 0.2 \times 10^{-3}$ $K^{-1}, \beta_o \rho_o = 0.8 \times 10^{-3} \times 1029$ psu^{-1} kg m^{-3}, $S_o = 35$ psu, and $c_w = 400$ J kg^{-1} K^{-1}.

$G1$ describes the generation and destruction of spatial density anomalies ($\bar{\rho}^{*2}$) through heat and freshwater fluxes at the sea surface. Note that $\frac{\delta[\rho_0]}{\partial z}$ is negative. $\bar{\rho}^{*2}$ are generated by a downward heat flux (positive $\bar{\mathcal{H}}^*$) or an excess of precipitation (positive $\bar{\mathcal{F}}^*$) over light water (characterized by negative $\bar{\rho}^*$), and destroyed when these fluxes occur over dense water (characterized by positive $\bar{\rho}^*$). $G3$ represents the generation of spatial density anomalies through time-mean vertical motions. $\bar{\rho}^{*2}$ are generated by upward motions in regions with dense water or downward motions in regions with light water. $G4$ describes how density flux of transients, $\overline{\rho' \mathbf{v}'}$, generates or destroys spatial density anomalies. $\bar{\rho}^{*2}$ are generated when the density flux $\overline{\rho' \mathbf{v}'}$ is in the direction of $\nabla \bar{\rho}^*$, and destroyed when $\overline{\rho' \mathbf{v}'}$ is in the opposite direction of $\nabla \bar{\rho}^*$.

D includes not only the effect of eddy diffusivity, but also processes related to spatial correlations between $\bar{\rho}^*$ and vertical advection of density. As the LSG model computes the advection of temperature and salinity using an upwind discretization method, which has a high inherent numerical diffusivity, the effect of diffusion is difficult to estimate. In the following, D will not be further specified, but treated simply as the residual of Eq. (11).

When using P_m as an approximation of the available potential energy of the time-mean circulation, $G1$ and $G2$ describe the generation and destruction of this energy through time-mean fluxes at the sea surface. $G3$ corresponds to the conversion between this energy and the kinetic energy of the time-mean circulation. $G4$ represents the conversion between the available potential energy of the time-mean circulation and that of the transients.

3 Effects of various processes on the three-dimensional density distribution in the ECHAM3-LSG integration

To assess the relative importance of various processes in generating and destroying spatial density anomalies, $G1$, $G2$, $G3$, and $G4$ and the global distributions of quantities related to $G1$–$G4$ are calculated from the ECHAM3-LSG integration. In the analysis given below, time means referred to averages over the integration period of 1000 years. Transients are defined as deviations from these averages. They represent variations on both seasonal and nonseasonal time scales. In the deep ocean, the latter represents essentially variations on time scales of decades to centuries.

3.1 The global integrals

Table 1 represents the global integrals of the generation and destruction of spatial density anomalies through the time-mean fluxes of heat and freshwater at the sea surface ($G1$ and $G2$), through the time-mean vertical motions ($G3$) and through the density fluxes induced by transients ($G4$). The values suggest that from a global point of view, spatial density anomalies are generated by the time-mean heat flux at the sea surface. All other processes ($G2, G3$, and $G4$) act to reduce spatial anomalies in the density fields. Furthermore, the amplitudes of $G1$ and $G3$ are of the order of 10^{11} W, whereas those of $G2$ and $G4$ are of the order of 10^{10} W. Thus, the generation of spatial density anomalies is, to a considerable extent, balanced by the destruction through vertical motions. To understand the processes behind these global integrals, spatial distributions of the responsible quantities are considered below.

3.2 The role of time-mean heat fluxes at the sea surface

The time-mean density anomalies in the first model layer ($\bar{\rho}_s^*$) have largest negative values in the tropics (Fig. 1). These anomalies increase poleward and become positive poleward of about 30°. The largest anomalies are located in the northern North Atlantic and in the Southern Oceans. The time-mean heat flux at the sea surface (Fig. 2a) acts to enhance the density contrast between the tropics and the high-latitude regions. This is done by downward heat fluxes (positive $\bar{\mathcal{H}}^*$) in the tropics where $\bar{\rho}^*$ is negative, and upward heat fluxes (negative $\bar{\mathcal{H}}^*$) in the northern North Atlantic and in the region north of the Antarctic where $\bar{\rho}^*$ is positive. Spatial density anomalies generated by these heat fluxes are indicated by maxima of positive values in Fig. 2b.

Table 1 Integrals G_1 to G_4, as defined in Eqs. (12)–(15). Units are 10^{10} W

G_1	G_2	G_3	G_4
46.55	−2.81	−39.86	−1.97

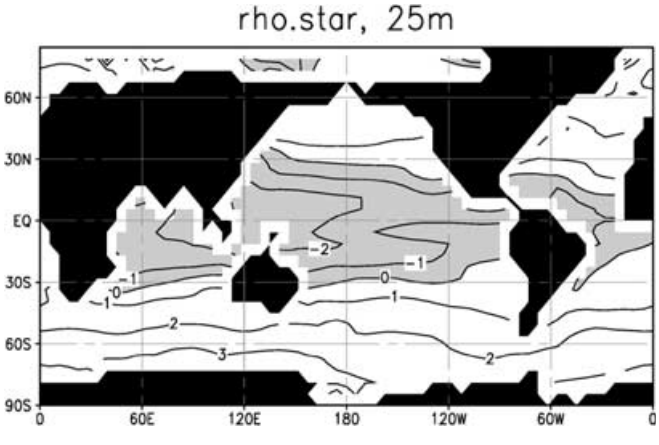

Fig. 1 Global distribution of time-mean spatial anomalies of density, $\bar{\rho}^*$, in the uppermost layer. Units are kg m^{-3}. Areas with negative values are *shaded*

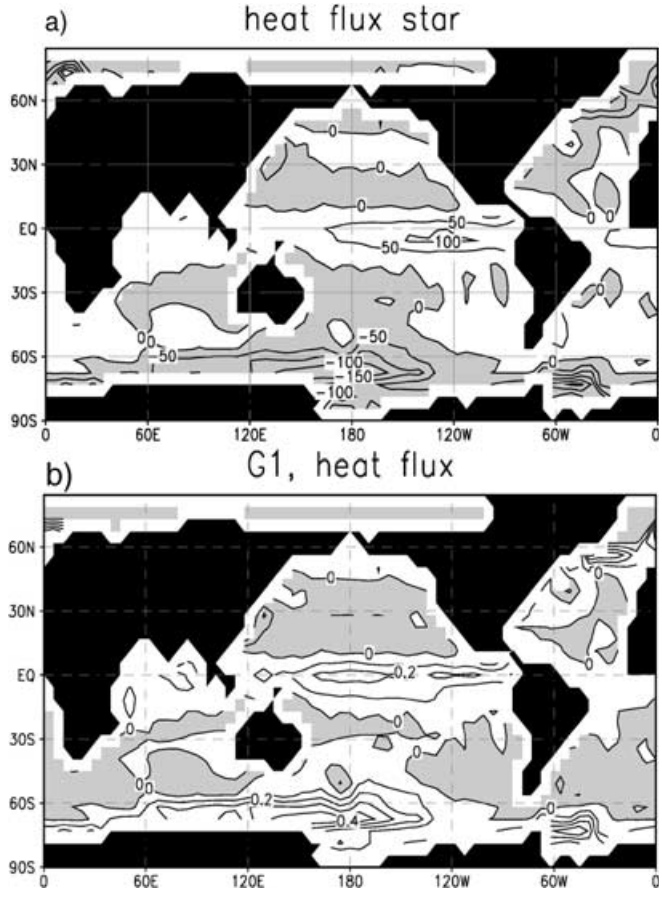

Fig. 2a, b Global distributions of **a** time-mean spatial anomalies of heat flux, $\bar{\mathcal{H}}^*$, and **b** the generation of density anomalies through $\bar{\mathcal{H}}^*$, $g\left(\frac{\delta[\overline{\rho_\theta}]}{\delta z}\right)_s^{-1}\frac{\alpha_o}{c_w}\bar{\rho}_s^*\bar{\mathcal{H}}^*$. The former is in W m^{-2} and the latter in 10^{10} W. *Shaded areas* indicate regions with negative fluxes (i.e., upward) in **a** and a destruction of spatial density anomalies in **b**

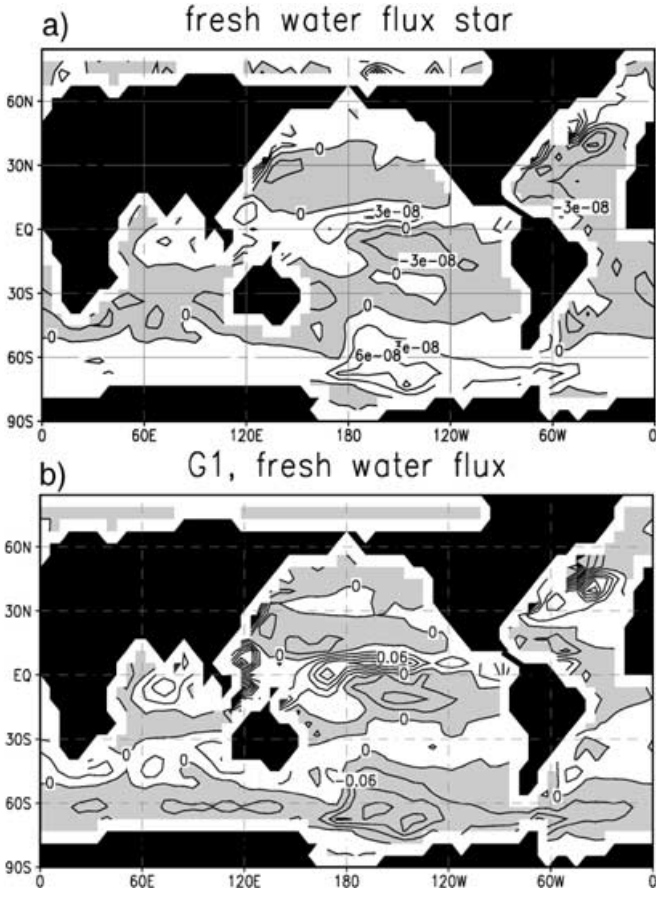

Fig. 3a, b Global distributions of **a** time-mean spatial anomalies of freshwater flux, $\bar{\mathcal{F}}^*$, and **b** the generation of density anomalies through freshwater flux, $g\frac{\delta[\overline{\rho\theta}]}{\delta z}_s^{-1}\beta_o\rho_o S_o\,\bar{\rho}^* s\bar{\mathcal{F}}^*$. The former is in m s^{-1} and the latter in 10^{10} W. *Shaded areas* indicate regions with negative fluxes (i.e., upward) in **a** and a destruction of spatial density anomalies in **b**

3.3 The role of time-mean freshwater fluxes at the sea surface

The effect of the time-mean freshwater flux on spatial density anomalies is shown in Fig. 3a and b. In most of the subtropical Pacific and Atlantic where negative $\bar{\rho}^*$ is found in Fig. 1, the ocean exports freshwater to the atmosphere ($\bar{\mathcal{F}}^*$ is negative). In the storm track regions where positive $\bar{\rho}^*$ is found, particularly in the northern North Atlantic and in the region south of 50°–60° S, the ocean receives freshwater from the atmosphere ($\bar{\mathcal{F}}^*$ is positive). These freshwater fluxes reduce latitudinal density differences and destroy spatial density anomalies (shaded areas in Fig. 3b). However, freshwater fluxes can also generate density anomalies. This is, in particular, the case in a narrow zonal band just north of the equator in the Pacific, where the ITCZ of the ECHAM atmosphere is located. In this region, precipitation dominates evaporation over relatively light water, making the water still lighter. A generation of density anomalies through freshwater fluxes is also found in the Atlantic between 30° and 45°N, where net evaporation occurs over relatively dense water. Table 1 shows that the net destruction dominates the net generation. Thus, from a global point of view, the freshwater fluxes act to reduce spatial density anomalies.

3.4 The role of time-mean vertical motions

In contrast to the fluxes of heat and freshwater which, according to Eq. (1), affect only density anomalies in the surface layer, vertical motions can alter density distribution not only in the surface layer, but also in the oceanic interior. Generally, the role of vertical motions changes from a weak productive one in the upper layers, where the wind-driven circulation dominates, to a strong destructive one in the deeper layers at 1000 to 4000 m, where thermohaline circulation prevails.

Consider first the situation in the surface layer. A comparison of the distribution of $\overline{\varpi}^*$ (Fig. 4a) with that of $\bar{\rho}^*$ (Fig. 1) shows that light water sinks in the subtropics and dense water rises in regions near 50°–60°.

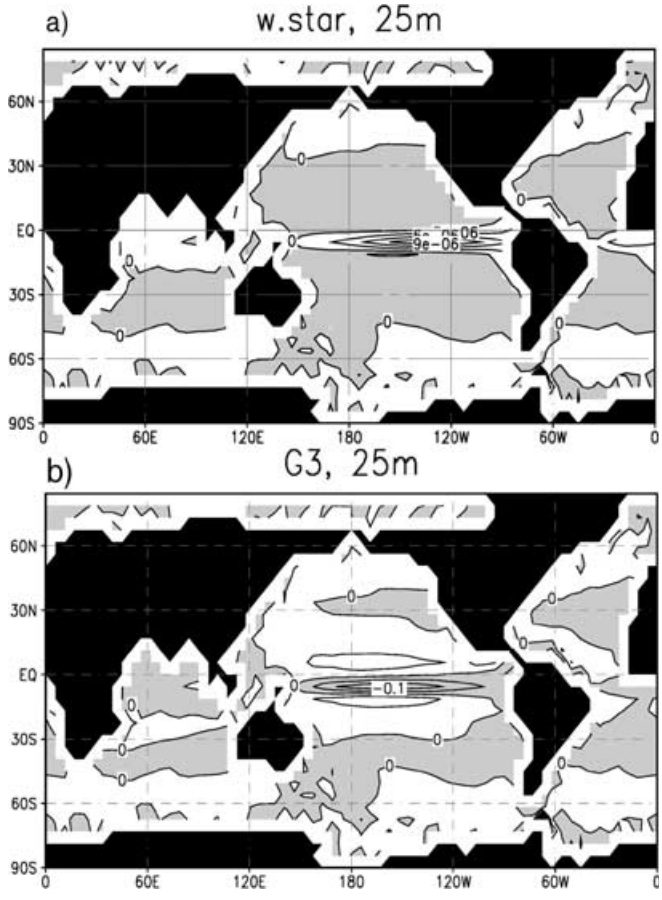

Fig. 4a, b Global distributions of **a** time-mean spatial anomalies of vertical velocity (*top*) in the uppermost layer and **b** $g\bar{\rho}^*\bar{w}^*$ (*bottom*) in the same layer. *Shaded areas* indicate regions with downward velocity in **a** and regions where spatial density anomalies are destroyed by vertical motions in **b**. $\bar{w}^*$ is in $\mathrm{m\,s^{-1}}$ and the conversion in 10^{10} W

These vertical motions lead to a generation of spatial density anomalies. A destruction is found in the equatorial regions, in particular in the equatorial Pacific, where density anomalies are reduced by strong upward motions (Fig. 4b). Apart from these equatorial vertical motions, the distribution of $\overline{w}^*$ coincides essentially with the distribution of the negative (positive) curl of zonal wind stress in the Northern (Southern) Hemisphere (not shown). Thus, extratropical vertical motions represent essentially the Ekman pumping induced by wind forcing. From an energetic point of view, the generation of spatial density anomalies through the extratropical vertical motions corresponds to a conversion of kinetic energy, which is generated by surface wind stress, into potential energy.

When integrated over the area of the surface layer, a net generation of spatial density anomalies through time-mean vertical motions is found. As demonstrated by the vertical profile of $g\bar{\rho}^*\bar{w}^*$ integrated over each model layer (Fig. 5), the productive role of vertical motions diminishes quickly with increasing depth. Below 150 m, a strong destruction of spatial density anomalies is found, with a maximum being located at 1000 to 2000 m.

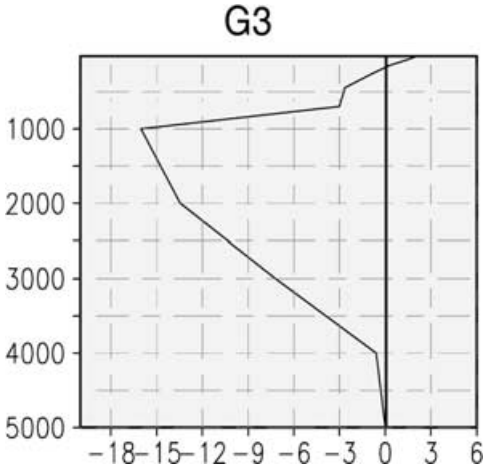

Fig. 5 Vertical profile of $g\bar{\rho}^*\bar{w}^*$. Unit is 10^{10} W

The destruction of density anomalies involves vertical motions which are part of the mean thermohaline circulation. At 1000 to 2000 m depth, the mean thermohaline circulation, as described by the zonally averaged streamfunction (von Storch et al. 2000), is related to downward motions in the North Atlantic and Southern Oceans, and upward motions in the Pacific and the Indian Oceans. Consistent with this, negative values of $\bar{w}^*$ are found in the North Atlantic and Southern Oceans (shaded areas in Fig. 6b) and positive values in the Pacific and the Indian Ocean (white areas in Fig. 6b). As the Atlantic and the Southern Oceans are more dense than the Pacific and part of the Indian Ocean (Fig. 6a), the vertical motions shown in Fig. 6b act to reduce the interbasin density contrast (shaded areas in Fig. 6c). From an energetic point of view, the reduction of global-scale density anomalies indicates a conversion of potential energy into kinetic energy through the time-mean thermohaline circulation.

3.5 The role of the time-mean density fluxes induced by transients

Similarly to vertical motions, density fluxes induced by transients can affect the density fields in the oceanic interior. When integrated over the each model layer, a destructive role of $\overline{\rho' v'}$ is found throughout the whole depth of the ocean. This is shown by negative values in Fig. 7. When decomposing the total variations (solid line, Fig. 7) into variations on seasonal (dashed) and nonseasonal (dotted) time scales, one finds that the reduction of spatial density anomalies through density fluxes associated with seasonal variations is significant only in the surface layer. Below 1000 m, the contribution from seasonal variations is negligible relative to that from nonseasonal low-frequency variations.

Furthermore, the process responsible for the reduction of spatial density anomalies through seasonal transients in the surface layer is different from that through nonseasonal variations in the deep oceans. For

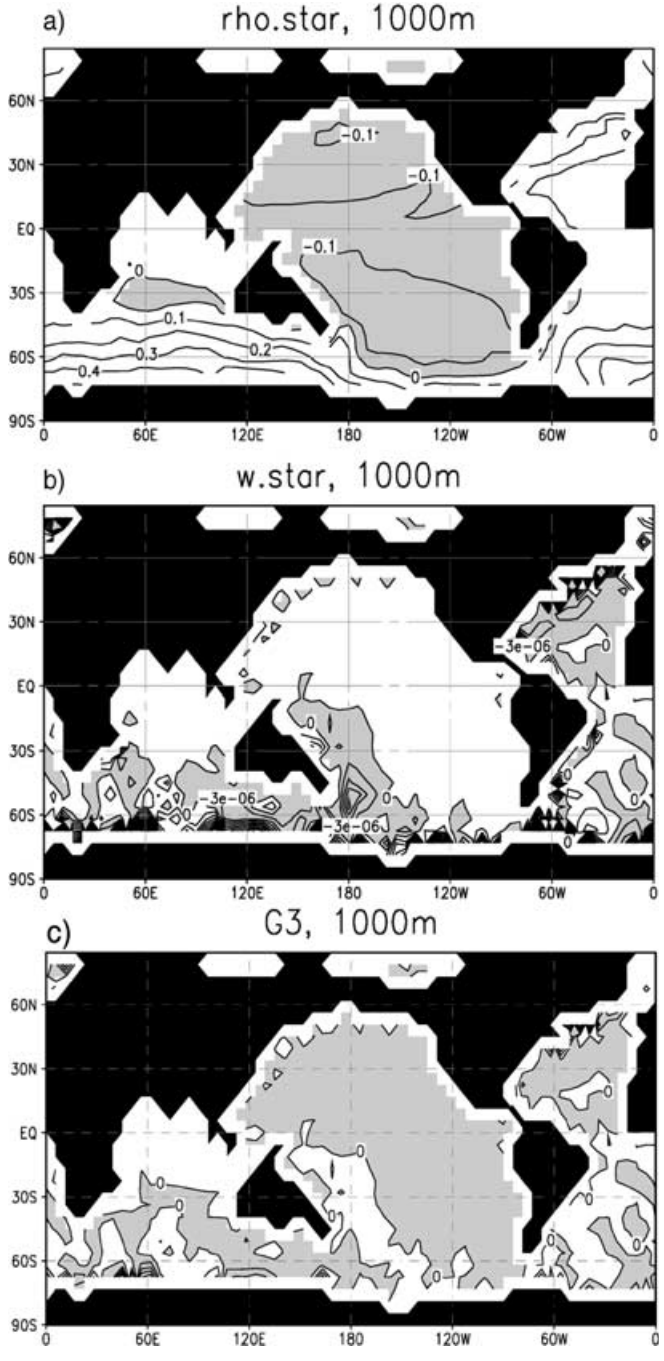

Fig. 6a–c Global distributions of time-mean values of **a** $\bar{\rho}^*$, **b** $\bar{w}^*$, and **c** $g\bar{\rho}^*\bar{w}^*$ in the layer at 1000 m depth. *Shaded areas* indicate regions with negative values. $\bar{\rho}^*$ is in kg m^{-3}, $\bar{w}^*$ in m s^{-1} and the quantity $g\bar{\rho}^*\overline{w}^*$ in 10^{10} W

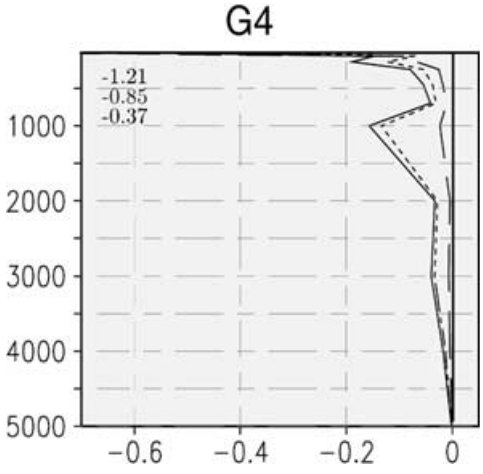

Fig. 7 Vertical profiles of $-g\left(\frac{\delta[\overline{\rho\theta}]}{\delta z}\right)^{-1}\overline{\rho'\mathbf{v}'}\nabla\cdot\bar{\rho}^*$. The contribution from the total transients (*solid line*) is decomposed into a part related to seasonal (*long-dashed*) and nonseasonal (*short-dotted*) variations. The *numbers* represent the total contribution (*top*), the seasonal (*middle*), and the nonseasonal (*bottom*) contribution in the uppermost layer. Units are 10^{10} W

the former, the most significant contribution of the reduction of P_m comes from the meridional density flux $\overline{\rho' v'}$, which represents the covariance between variations of ρ and v on seasonal time scales (Fig. 8a). In the region from about 25°S to 20°N, where trade winds prevail, positive values of $\overline{\rho' v'}$ are found in the Northern Hemisphere and negative values of $\overline{\rho' v'}$ in the Southern Hemisphere. Poleward of this tropical region, where westerlies prevail, a band of equatorward density flux is found in each hemisphere. These zonally oriented structures indicate that the meridional density fluxes result essentially from the meridional Ekman transports induced by the seasonally varying zonal wind stresses at the sea surface. As the annual cycle is most pronounced in the Northern Hemisphere, the equatorward density fluxes have larger amplitude in the North Pacific and North Atlantic than in the southern oceans.

The meridional gradient of $\bar{\rho}^*$ in the uppermost layer is shown in Fig. 8b. In the Northern Hemisphere, poleward density fluxes are, to a large extent, located in regions where the meridional gradient of $\bar{\rho}^*$ is negative and equatorward fluxes in regions where the meridional gradient of $\bar{\rho}^*$ is positive. The opposite is found in the most of the Southern Hemisphere. As these meridional density fluxes are down the density gradient, spatial density anomalies are reduced (shaded areas in Fig. 8c).

The density fluxes of transients on seasonal time scales account for only about one half of the value of *G4* given in Table 1. The other half results from transients on nonseasonal time scales in the oceanic interior (short-dashed line in Fig. 7). As pointed out in the Introduction, these transients represent variations on time scales from decades to centuries excited by fluctuating surface forcing. Large contributions come from the vertical density flux $\overline{\rho' w'}$ in the interior at 1000 m depth.

The situation at 1000 m depth is shown in Fig. 9. The vertical density flux due to nonseasonal transients is upward in the Pacific and the Indian Oceans, but downward in the North Atlantic and in the region north of the Antarctic (Fig. 9a). On the other hand, the vertical gradient of $\bar{\rho}^*$ (Fig. 9b) is positive in the Atlantic and the southern Indian Oceans and negative in the Pacific and the subtropical Indian Oceans. That is, relative to the mean density $[\bar{\rho}]$, the density decreases with depth in the Atlantic and the southern Indian Oceans, but increases

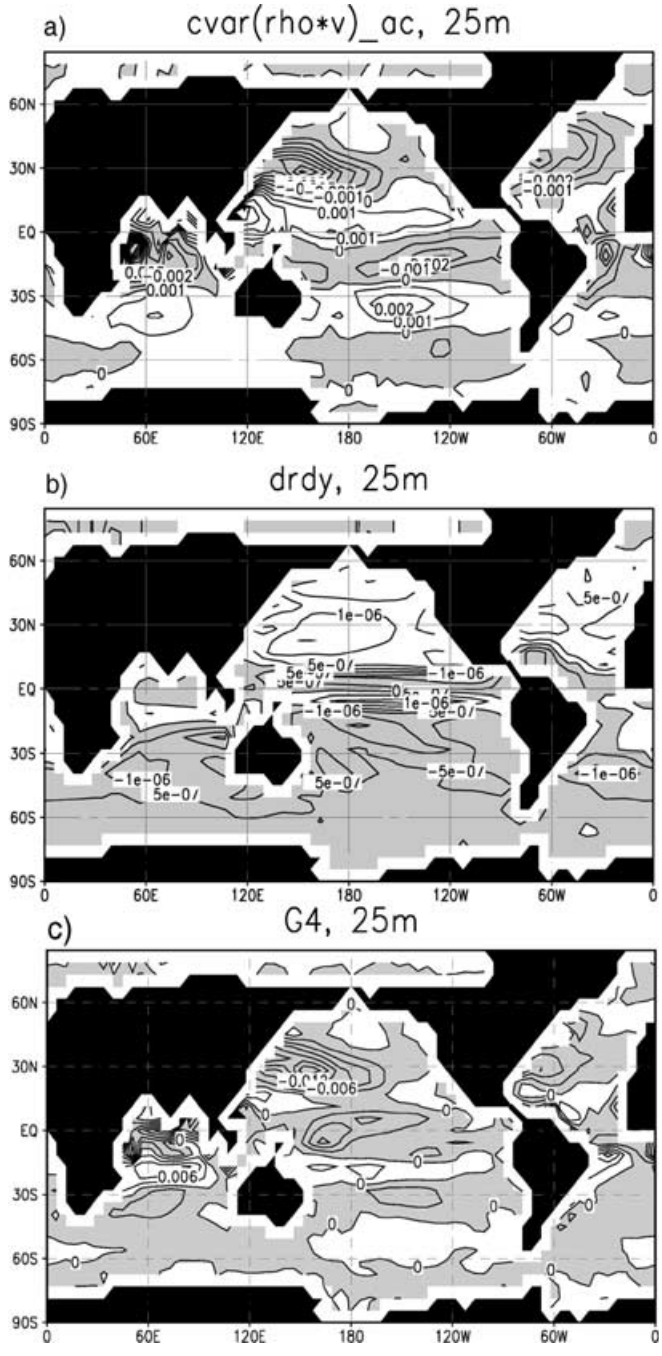

Fig. 8a–c Global distributions of **a** $\overline{\rho' v'}$, **b** the meridional gradient of $\bar{\rho}^*$, and **c** $-g\left(\frac{\delta[\overline{\rho\theta}]}{\delta z}\right)^{-1}\overline{\rho' \mathbf{v}'} \nabla \cdot \bar{\rho}^*$ for the uppermost layer. *Shaded areas* indicate regions with negative values. Units are, respectively, kg m^{-2} s^{-1}, kg m^{-4}, and 10^{10} W

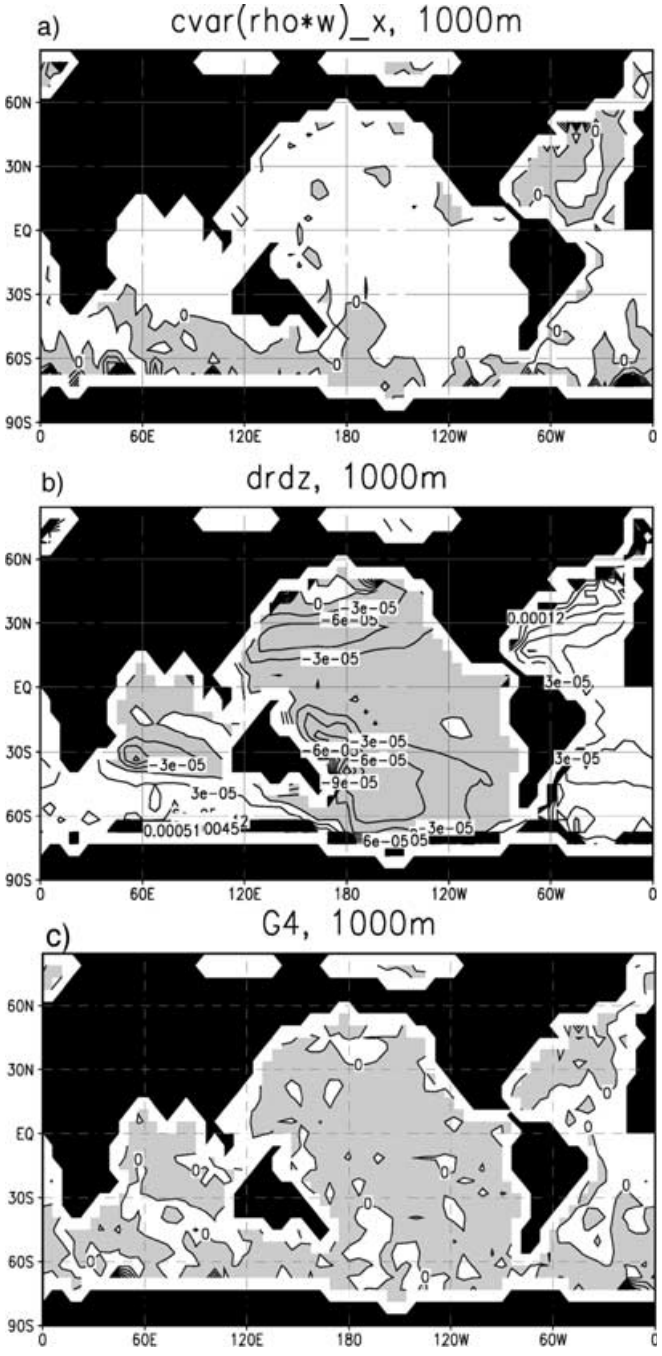

Fig. 9a–c Global distributions of the following three quantities in the layer at 1000 m: **a** $\overline{\rho' w'}$, **b** the vertical gradient of $\bar{\rho}^*$, and **c** $-g\left(\frac{\delta[\overline{\rho\theta}]}{\delta z}\right)^{-1}\overline{\rho' \mathbf{v}'} \nabla \cdot \bar{\rho}^*$. *Shaded areas* indicate regions with negative values. Units are, respectively, kg m^{-2} s^{-1}, kg m^{-4}, and 10^{10} W

with depth in the Pacific and the subtropical Indian Oceans. This indicates that the Pacific and the Indian Oceans are more stable when compared with the Atlantic and the most part of the Southern Oceans. The vertical density fluxes shown in Fig. 9a act to reduce this interbasin density difference. By doing so, density anomalies are reduced on a global scale (shaded areas in Fig. 9c).

4 Conclusions and discussions

4.1 Conclusions

The effects of four processes on the three-dimensional time-mean density distribution are assessed using the ECHAM3-LSG integration. The results suggest that the

maintenance of the three-dimensional density anomalies involves the generation through the time-mean surface heat flux on the one hand, and the destruction through the time-mean surface freshwater flux, time-mean vertical motions, and interior density fluxes of transients on the other.

The generation operates through the differential heating at the surface that makes light tropical water lighter and dense water in the northern North Atlantic and north of the Antarctic more dense. Most of such generated density anomalies are destroyed through the time-mean vertical motions in form of sinking of relatively dense water in the North Atlantic and the Southern Oceans and rising of less dense water in the Pacific and Indian Oceans. These vertical motions effectively reduce the density differences in the oceanic interior. When integrated over the entire volume of oceans, the reduction through this process is of the same order as the generation through the time-mean surface heat flux. In addition to this process, spatial density anomalies are further reduced, though to a much smaller extent, by the time-mean freshwater flux at the sea surface and by the interior density fluxes associated with transients. The former results essentially from the freshening (excess of precipitation over evaporation) over the northern North Atlantic and the Southern Oceans. The latter can be split into contributions from density fluxes induced by seasonal and nonseasonal variations. The annual cycle in zonal surface momentum fluxes leads to meridional Ekman transports and hence meridional density fluxes. These fluxes act to reduce the meridional gradient of the time-mean density distribution in the surface layer. The other contribution comes from low-frequency variations in the oceanic interior. These transients organize themselves in such a way that the associated density fluxes systematically stabilize the water in the northern North Atlantic and in the region north of the Antarctic and destabilize the water in the Pacific and the Indian Ocean. Due to these vertical density fluxes, the existing density differences between different ocean basins are further reduced.

When P_m is considered as an approximation for the available potential energy of the time-mean circulation, the above results can be interpreted as the following. The time-mean heat flux at the sea surface is the source, while the other processes are sinks of the available potential energy. P_m generated by the heat flux is partly destroyed by the time-mean fresh water flux, partly converted into kinetic energy of the time-mean circulation through vertical motions, and partly converted into available potential energy of the transients through the interior density fluxes.

4.2 Implication for the stability of the thermohaline circulation

By adding extra amounts of freshwater into the North Atlantic, Mikolajewicz and Maier-Reimer (1994) and Schiller et al. (1997) studied the stability of the LSG ocean in an ocean-only mode using climatological fluxes and in a coupled mode. They found the thermohaline circulation in the coupled model responses less sensitive to additional changes in the external forcing and more stable relative to that in the ocean-only model. They suggested a few stabilizing processes. Another explanation could be that the coupled model generates surface fluxes that contain not only a time-mean component, but also a fluctuating one, which excites variations in the oceanic interior. The associated density fluxes contribute to a reduction of interbasin density differences and lead to a more stable density distribution and thereby to a more stable thermohaline circulation. Clearly, further studies are required to clarify the role of externally excited variations on the stability of thermohaline circulation.

4.3 Other model estimates of the role of vertical motions

Oort et al. (1994) considered a few model estimates of the $G3$ term. They found that the sign of $G3$ depends on the strength of the lateral diffusion of heat relative to other diffusions. $G3$ tends to be negative for a weak, but positive for a strong horizontal diffusion of heat. The present study considers only one integration and is therefore unable to answer the question of whether similar dependence will also be produced by the LSG model. However, the analysis does indicate why the role of vertical motions changes with varying strength of the diffusion of heat.

It has been shown that density anomalies are mainly generated through the heat flux at the sea surface. This generation cannot be balanced by the freshwater flux at the sea surface, as the latter is 1 order of magnitude smaller than the former. A similar result was obtained by Oort et al. (1994) using observational data. There are two ways to balance this generation of spatial density anomalies. First, the generation can be directly balanced by the diffusion of heat. This happens when the diffusion of heat dominates that of momentum. In this case, a positive $G3$ is required. This is because the generation of kinetic energy through the surface wind stress also has to be balanced. As the diffusion of momentum is weak, a balance is only possible through vertical motions that convert kinetic energy into potential energy, resulting in a positive $G3$. Secondly, the generation of density anomalies through heat flux can also be balanced by a negative $G3$. This happens when the diffusion of momentum dominates the diffusion of heat. Instead of being directly dissipated through diffusion of heat, density anomalies are reduced through vertical motions that convert potential energy into kinetic energy, which is subsequently dissipated through the strong diffusion of momentum. This is the case found in the ECHAM3-LSG integration.

Generally, given a realistic surface forcing (which is ensured by the flux corrections in the ECHAM3-LSG

integration), the heat and freshwater fluxes at the sea surface result in a net generation of spatial density anomalies. This generation can be balanced in different ways, depending on the relative strengths of diffusions implemented in the model. The present study describes only the situation in the oceans produced by the ECHAM3-LSG model. For the understanding of the establishment of the mean density distribution and the resulting maintenance of the global thermohaline circulation in the real world, one needs improved AO-GCMs which resolve the bulk of oceanic eddies so that the strength of diffusions can be significantly reduced. In addition to this, analyses of model integrations need to be carefully carried out. Such analyses can be powerful, when they are performed within a proper theoretical framework. Here, an equation of density variance is used as a theoretical basis. One can also study the density distribution within the framework of the full energy cycle, thereby using a more correct definition of the available potential energy (Huang 1999). Such an analysis will be more complete and should be considered in future work.

Acknowledgements I thank Ulrich Cubasch and his colleagues for providing me with the ECHAM3/LSG integration, Peter Müller and Richard Greatbatch for valuable suggestions.

References

Delworth TL, Greatbatch RJ (2000) Multidecadal thermohaline circulation variability driven by atmospheric surface flux forcing. J Climate 13: 1481–1495

Hasselmann K, (1976) Stochastic climate models. Part I: Theory. Tellus 28: 473–485

Huang RX (1998) Mixing and available potential energy in a Boussinesq ocean. J Phys Oceanogr 28: 669–678

Maier-Reimer E, Mikolajewicz U, Hasselmann K (1993) Mean circulation of the Hamburg LSG OGCM and its sensitivity to the thermohaline surface forcing. J Phys Oceanogr 23: 731–757

Mikolajewicz U, Maier-Reimer E (1994) Mixed boundary conditions in ocean general circulation models and their influence on the stability of the model's conveyor belt. J Geophys Res 99: C11, 22633–22644

Oort HA, Ascher SC, Levitus S, Peixoto JP (1989) New estimates of the available potential energy in the world ocean. J Geophys Res 94: 3187–3200

Oort HA, Anderson LA Peixoto JP (1994) Estimates of the energy cycle of the oceans. J Geophys Res 99: 7665–7688

Rahmstorf S (1995) Bifurcation of the Atlantic thermohaline circulation in response to changes in the hydrological cycle. Nature 378: 145–149

Schiller A, Mikolajewicz U, Voss R (1997) The stability of the North Atlantic thermohaline circulation in a coupled ocean–atmosphere general circulation model. Clim Dyn 13: 325–347

Stocker TF, Wright DG (1991) Rapid transitions of the ocean's deep circulation induced by changes in surface water fluxes Nature 351: 729–732

Stommel H (1961) Thermohaline convection with two stable regimes of flow. Tellus XIII; 224–230

UNESCO (1981) Tenth report of the joint panel on oceanographic tables and standard. UNESCO. Tech Paper Mar Sci 36: 25 pp

von Storch J-S, Müller P, Stouffer RJ, Voss R, Tett SFB (2000) Variability of deep-ocean mass transport: spectral shapes and spatial scales. J Climate 13: 1916–1935

von Storch J-S, Müller P, Bauer E (2001) Climate variability in millennium integrations with coupled atmosphere–ocean GCMs. A spectral view. Clim Dyn 17: 375–389

Voss R (1996) Entwicklung eines Kopplungsverfahrens zur Reduzierung der Rechenzeit von Atmosphäre-Ozean-Modellen. Max-Planck-Institut für Meteorologie, Hamburg, Examensarbeit 38 (ISSN 0938-5177), 123 pp

Voss R, Sausen R Cubasch U (1998) Periodically synchronously coupled integrations with the atmosphere–ocean general circulation model ECHAM3/LSG. Clim Dyn 14: 249–266